Fuel Sensitivity of Lean Blowout in a RQL Gas Turbine Combustor

C. Thomas Wey
NASA Glenn Research Center, OH 44135

Abstract

Transition from fossil fuels to synthetic drop-in fuels without the need to change existing combustors is the current research topic. The combustor performances such as cold-day ignition limits, lean blow-out (LBO) limits and altitude relight limits are the main focus points. The objective of this work is to evaluate the effect of different fuel candidates on the operability of gas turbines by comparing a conventional petroleum-based fuel with one other alternative fuel candidate. Time filtered Navier-Stokes simulations (TFNS) and K-LES are performed to examine the performance of these fuels at the stable conditions close to blow-out in a referee combustor rig.

Introduction

Recent more stringent emission standards have enticed the development of more fuel-efficient and low-emission combustion system for aircraft gas turbine applications. There is also interest in producing "alternative jet fuels" from various non-petroleum sources that consist solely of hydrocarbons and that provide essentially identical performance to that from petroleum-derived jet fuels. However, the cost is high to develop the technical data for the acceptance of the fuel standards. While these alternative jet fuels must meet current requirements for key parameters such as heat release, there are many other factors to be examined before accepting each alternative jet fuel for aviation use, including combustor operability characteristics, such as lean blowout (LBO), cold start, and high-altitude relight. In the present work, simulations of the approach to lean blow-out for a conventional and an alternative jet fuel are performed and analyzed for a single-cup, swirl-stabilized RQL (rich-burn, quick-mix, lean-burn) combustor [1]. This RQL combustor is the Referee Rig for the National Jet Fuels Combustion Program (NJFCP) [2] which has performed LBO tests for a number of conventional and alternative jet fuels. The two fuels considered are an average jet fuel (denoted as "A2" in the NJFCP) and a test fuel (C1) consisting of 100% Gevo ATJ fuel, which contains highly branched C12 and C16 paraffin and will distillate 80% of its components at temperatures less than 200°C (while A2 requires temperatures of 230°C or above to distillate 80% of its components)[3].

The objective of the present work is to compare the results obtained from the TFNS (time filtered Navier-Stokes) and LES simulations with the experimental data [1]. The open source version (OpenNCC) of National Combustion Code (NCC) currently under-development at NASA Glenn Research Center will be used for the calculations. OpenNCC adopts the data structure of arbitrary polyhedrons that permit cells of arbitrary shape to be used: cells can have an arbitrary number of faces and faces can have an arbitrary number of points. A brief summary of the code is listed here. The code solves the compressible Navier-Stokes equation while the preconditioning is optional for simulating the low Mach number flow. A second order accurate central or upwind scheme is used for spatial discretization of the Euler fluxes in TFNS or LES governing equations. A third order accurate central or upwind scheme is available as well via Taylor series expansion for spatial discretization of the Euler fluxes. For a typical spray reacting simulation, the third order SLAU2[4] flux splitting method for the inviscid flux requires 40 percent more computer-time compared against that of the second order SLAU2 scheme. A second order accurate central scheme is used for discretization of the Laplacian terms in the governing equations. For the temporal integration, the options include: (1) non-iterative second order predictor-corrector MacCormack scheme; (2) non-iterative global-time-step multi-stage Runge-Kutta scheme; (3) dual-time sub-iterative 3-4-5-stage Runge-Kutta scheme. Four available turbulence models in the code are summarized in Table 1 from the coding point of view.

Turbulence Model	Turbulence Stresses	Eddy Viscosity	K-Destruction Term	Coefficients
TFNS	Quadratic & Cubic	$C_\mu \rho K^2/\varepsilon$	$\rho\varepsilon$	RCP: Prescribed
K - LES	Linear	$C_\nu \rho K^{0.5}\Delta$	$C_\varepsilon \rho(K)^{1.5}/\Delta$	C_ν, C_ε: Prescribed or computed by LDKM scheme
LES	Linear	$(C_s\Delta)^2\rho\|S\|$	N/A	C_s, Prescribed
TFNS/LES	Quadratic & Cubic	Min($C_\mu \rho K^2/\varepsilon$, $(C_s\Delta)^2\rho\|S\|$)	Max($\rho\varepsilon$, $C_\varepsilon \rho(K)^{1.5}/\Delta$)	RCP: Prescribed C_ε, C_s: Prescribed

Table 1 Turbulence Models in the code.

The liquid spray solver is based on a Lagrangian scheme and various well-established models for droplet drag; the Frossling[5] and Faeth[6] vaporization models coupled with the constant droplet internal heating and it employs models for gas-film valid over a wide range of low to intermediate droplet Reynolds numbers.

Results and Discussion

A patched mesh of 12,640,138 hexahedrons (provided by UTRC through Ga Tech) was acquired to study approach to lean blowout for this combustor. The mesh is patched together by nine blocks. The mesh resolutions are not too compatible between blocks. The interface among the blocks is mainly achieved by linear interpolation of the primitive variables.

The injection system consists of two outer axial swirlers and an inner radial swirler with a pressure-swirl atomizer nested in the center (See Figure 1). The atomizer and the radial swirler are located upstream of the exit plane of the axial swirlers. Dilution holes are located at two axial positions along upper and lower walls of combustor with three holes at the first row (45mm downstream of the injector exit plane), and four holes at the second row further downstream. The LBO tests start at a stable flame condition near LBO (2.07 atm combustion chamber pressure and overall equivalence ratio of 0.096) and the lower the fuel flow rate in controlled and repeatable manner until LBO occurs (determined by the rapid drop of the signal from a photodiode directed at the combustor primary zone). The average time required to ramp the fuel down to LBO during actually testing was typically 200-300 sec.

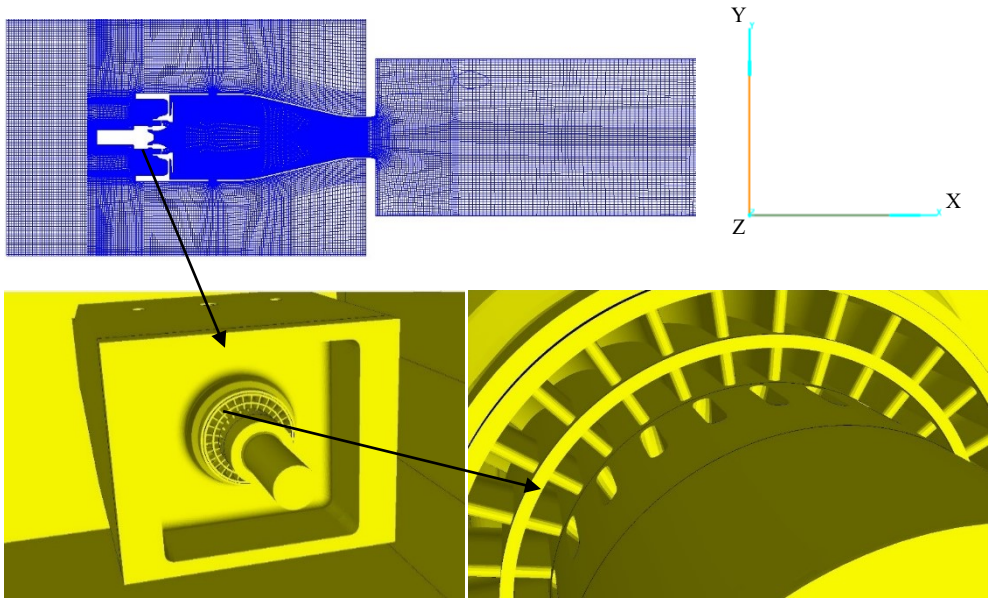

Figure 1 A middle plane cut of the patched grid. Number of elements is 12,640,138 hexahedrons. Injection system consists of two outer axial swirlers and an inner radial swirler. The resolutions of the meshes between the patched grids are barely compatible.

Case 1. Non-reacting flow simulations: all liner and dome flows are modelled by uniform effusion cooling

A represented plot of the grid is shown in Figure 1. A non-reacting flow simulation is conducted using the following boundary conditions. At the inlet, the mass flow rate is 0.3914 kg/s, the static temperature is 394 K. The back pressure at the exit of the extended outlet block set to 207,000 Pa. All walls are no-slip and adiabatic.

All dilution holes and the three swirlers are gridded by the patched grids, some interface boundary conditions are needed. At the moment, only simple interpolations of the primitive variables are conducted for the patched grids and there is no effort yet to make them satisfying interface flux conservations. Therefore, it is quite noticeable that the mass is not fully conserved across the patch-grid interfaces, particularly for the reacting cases because of elevated dynamics of the pressure.

The uniform effusion cooling conditions at the combustor dome are 3.216 kg/s per m^2 (0.0250 kg/s) and 394 K on one side of the walls and -5.3802 kg/s per m^2 (-0.0250 kg/s) on the other side of walls since the size of wall areas are different.

Similarly, the uniform effusion cooling conditions at: (1) the forward liner are 3.1608 kg/s per m^2 (0.04188 kg/s) and 394k versus -1.6618 kg/s per m^2 (-0.04188 kg/s) and 394 K, (2) the middle liner are 2.92 kg/s per m^2 (0.04266 kg/s) and 394 K versus -2.3797 kg/s per m^2 (-0.04266 kg/s)and 394 K, (3) the aft liner are 2.2679 kg/s per m^2 (0.06575 kg/s) and 394 K, versus -1.8867 kg/s per m^2 (-0.06575 kg/s) and 394 K, (4) the side slot liner are 46.53 kg/s per m^2 (0.06575 kg/s) and 394 K versus -46.53 kg/s per m^2 (- 0.06575 kg/s) and 394 K. For simplicity, in the current work, the mass flow from the side slot liner has been folded into the aft liner. The total mass flow rate for the entire combustor is 0.3914 kg/s after in and out cancellations for the film-cooling boundary conditions. The boundary conditions used are the same as those of the benchmark operating conditions for the AFRL referee rig.
From Figures 2 to 5, the contours of TFNS speed, x-velocity, y-velocity and pressure are shown respectively. It is observed that the recirculation zones are quite noticeable due to the primary and the secondary dilution jets. However, the jet bending due to the dilution is less noticeable due to the liner flow diversion that is not gridded. Though the jet bending is symmetric.

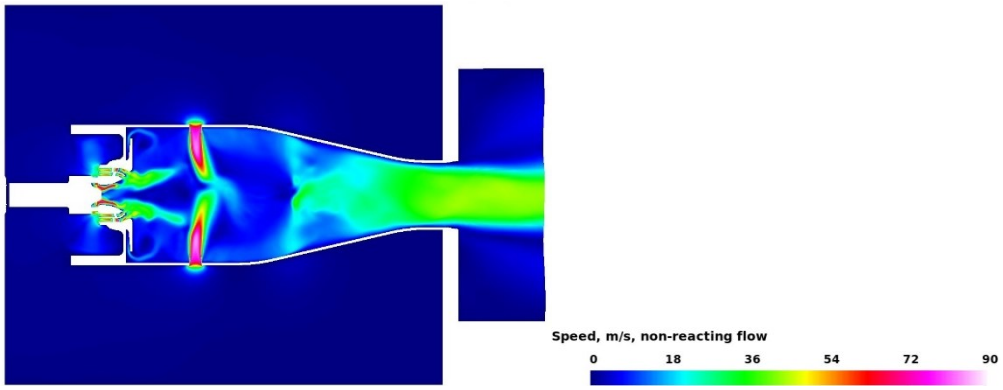

Figure 2 A middle z plane cut of the speed for the non-reacting flow.

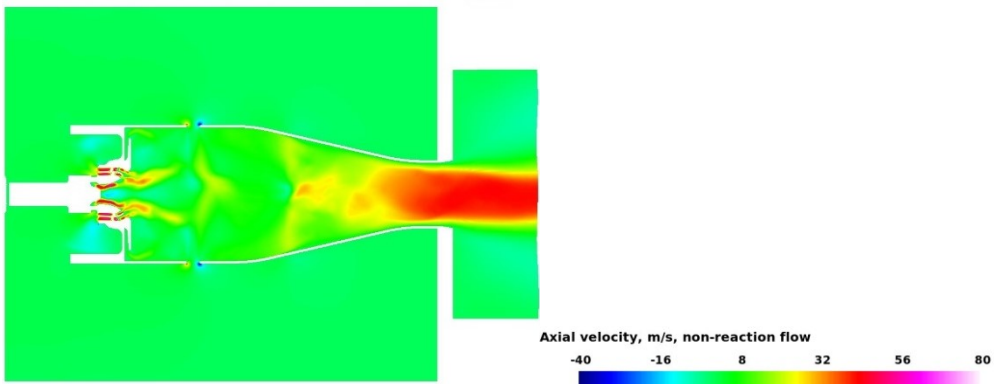

Figure 3 A middle z plane cut of the axial velocity for the non-reacting flow.

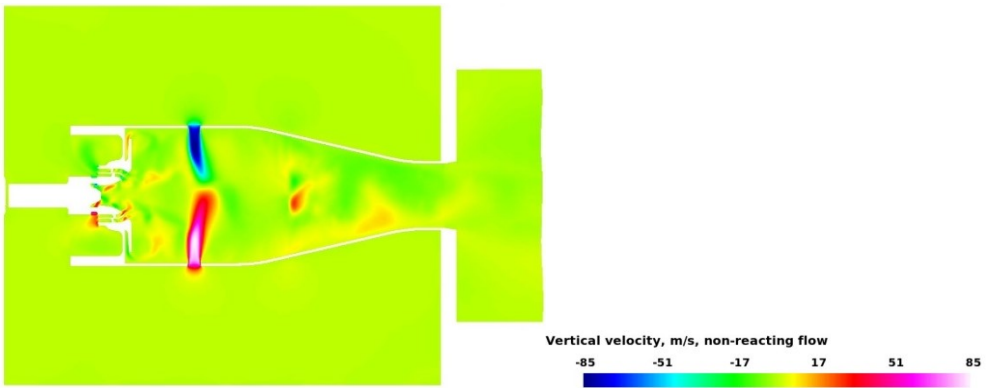

Figure 4 A middle z plane cut of the y-velocity for the non-reacting flow.

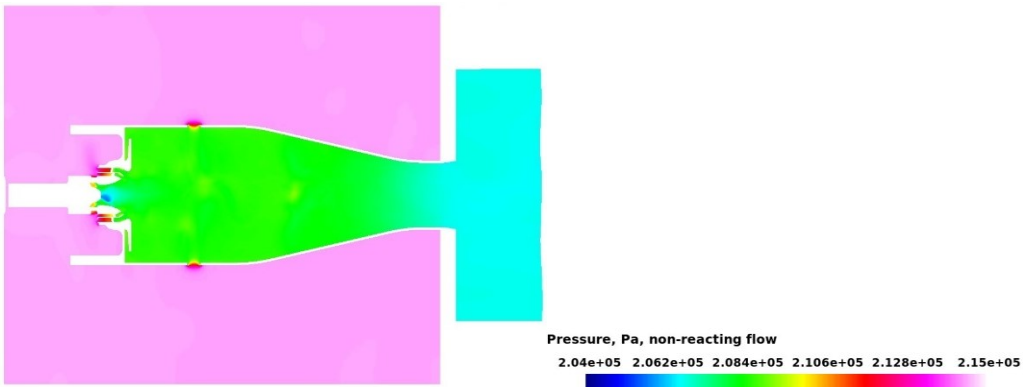

Figure 5 A middle z plane cut of the pressure for the non-reacting flow.

The flow split between the three swirlers and the two rows of the dilution holes is computed and compared to the experimental measurements. The locations of the mass flow split computed by the code are shown in Figure 6. However, the experimental data are obtained by blocking all components except the particular component whose data is to be collected. The results are listed in Table 2. The computed mass flow rates are the results of TFNS option. For the each of the three swirlers, the relative error of the mass flow rate is more than 10 percent. The overall relative error of the mass flow rates for the whole swirlers is around 7 percent. It is because the patched surfaces between the swirlers and the forward combustor are poorly defined. This reason plus the lack of the flux conservation of the boundary conditions for the patched grids is the main cause of the high errors. The relative errors of the mass flow for the two rows of the dilution holes are much smaller. It is because the patched surfaces between the aft-inlet component and the forward and aft combustors are flat and well defined.

Non-reacting flow split	EXP, kg/s	TFNS, kg/s	Error =(TFNS-EXP)/EXP
Exit of Radial swirler	0.0143	0.0112	-21%
Exit of Axial inner swirler	0.0189	0.0208	10%
Exit of Axial outer swirler	0.0246	0.0302	22%
Exit of all swirlers	0.0578	0.0622	7%
Exit of Dilution row 1	0.0395	0.0382	-3%
Exit of Dilution row 2	0.0454	0.0409	-10%

Table 2 Comparison of measured and computed mass flow rates for the swirlers and the dilution rows.

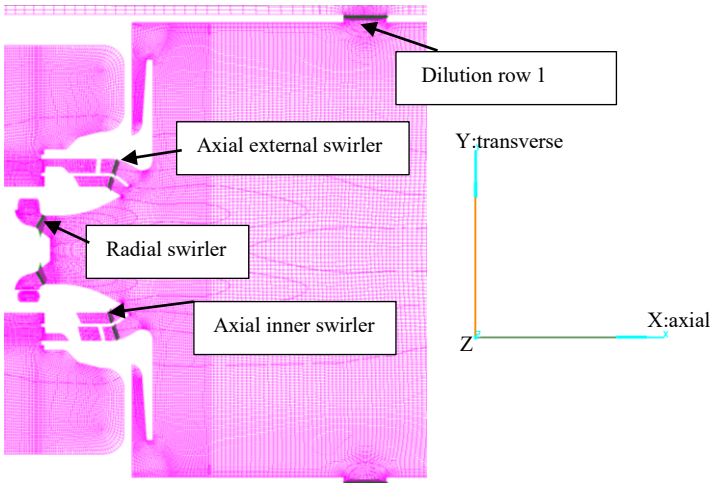

Figure 6 Locations of the mass flow split computed by the code.

Case 2. Reacting flow simulations: Cat-A2 as the fuel

The air related boundary conditions used in this case are the same as Case 1.

The averaged formula of the Cat-A2 (Designation of POSF11498) is represented by $C_{11.4}H_{21.7}$.

A reduced hybrid chemistry (Hychem) model[8] is used for the mechanism of the real Cat-A2 fuel. The non-stiff version of the reduced mechanism consists of 31 species and 202 reactions for the purpose of lowering the cost of the finite chemistry simulations.

The liquid properties are prescribed from T. Edward experimental database [4] that includes the density, heat capacity, viscosity and latent heat of vaporization, shown in Table 3. The gas properties are prescribed from H. Wang's HyChem model [8].

The first overall equivalence ratio selected for Cat-A2 fuel is 0.096 for the stable operating condition. The spray boundary conditions applied are briefly described here. The liquid boundary conditions are created such that at 2 mm downstream of the physical fuel injector, there are six rings of distinguished spray droplets formed. Each ring has its (1) cumulative distribution function, (2) inner and outer injection angles of the ring, (3) represented SMD computed from CDF as a reference, (4) particle speed, (5) mass flow rate

of the spray. The actual values are listed in Figure 7.

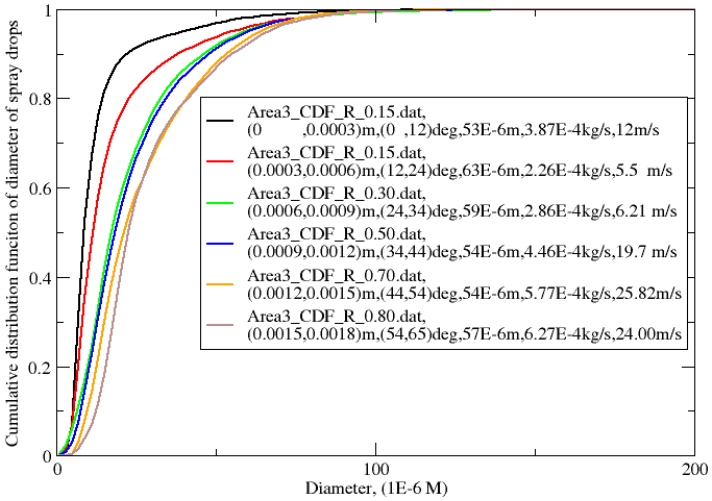

Figure 7 CDF from Purdue PDPA spray measurements and spray boundary conditions.

Liquid Physical Properties	Units	Cat-A2	Cat-C1
Density	Kg/M^3	-0.74617*T+1018.26	-0.72*T+967.01
Heat Capacity	J/Kg/K	4.28*T + 723.0	4.10*T+753.0
Viscosity	Pa-S	0.08949*exp(-0.01394*T)	1.89212*exp(-0.02393*T)
Vapor Pressure	Pa	10.**(28.95-3000.4/T-6.5*log10(T)-0.0004*T)	10.**(28.9-3000.4/T-6.5*log10(T)-0.0004*T)
Latent Heat	J/Kg	$380000*[(T_c-T)/(T_c-298]^{0.375}$	$360000*[(T_c-T)/(T_c-298]^{0.375}$
Critical Temperature	K	760.4	740.2

Table 3 Liquid physical properties fitted in terms of temperature.

A middle slab cut of time-averaged axial velocity and averaged axial recirculation velocity are shown in the left and right panels of Figure 8. In Figure 9, the time-averaged transverse velocity on a middle slab cut Is shown. The bending of the dilution jets is noticeable.
From Figures 10 to 12, the contours of time-averaged K-LES speed, pressure and temperature in a central slab cut normal to the z axis are shown respectively. The higher speed accelerated in the exit area of the aft-combustor could be contributed due to the chemical mechanism used. The pressure distribution in the aft-combustor compartment is quite uniform. The temperature distribution in the combustor is somewhat unsymmetrical and one higher temperature zone exists in lower portion of the combustor. The values of the temperature drop very quickly from the first row of the dilution hole to the second row of the dilution hole. The time-averaged C1 mass fraction is shown in Figure 13. It shows that the injected liquid fuel is mainly vaporized in the swirler cup due to well organized recirculation zone shown in the right panel of Figure 8. The time-averaged OH mass fraction and experimentally measured OH* PLIF are shown in Figure 14.

Temporal efficiency of A2 fuel evaporations of five various equivalence ratios are shown in Figure15. The base line equivalence ratio is 0.096 which is recorded from 10 MS to 42 MS. When time is at 26 MS, a new simulation with the equivalence 0.078, which is stepped down from 0.096, has started while the 0.096 simulation is continuing. At 28 MS, 0.082 and 0.082 simulations, which are stepped up from 0.078, have begun while 0.096 and 0.078 simulations are continuing. At 38 MS, another new simulation with 0.088 equivalence ratio starts while others are continuing.

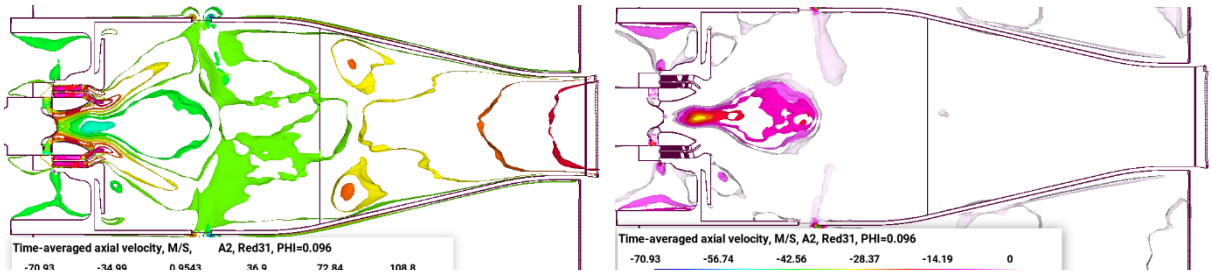

Figure 8 A middle slab cut of time-averaged axial velocity and time-averaged axial recirculation velocity.

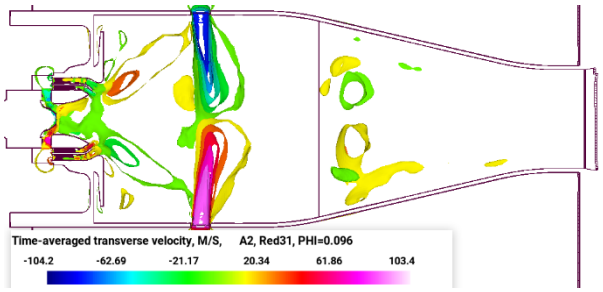

Figure 9 A middle slab cut of time-averaged transverse velocity.

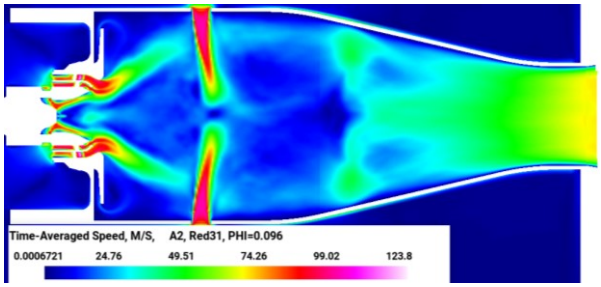

Figure 10 Time-averaged velocity magnitude in a central z-normal cut plane.

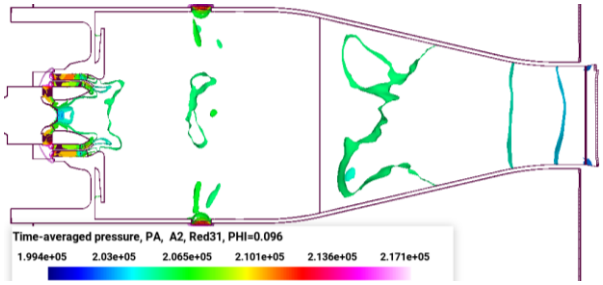

Figure 11 A middle slab cut of time-averaged pressure.

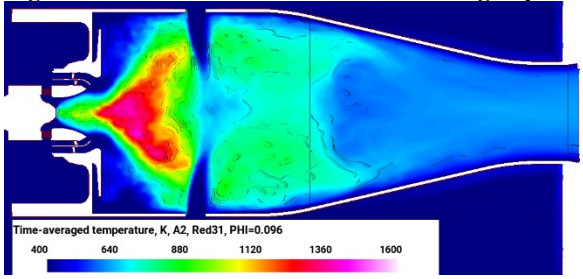

Figure 12 A middle plane and slab cut of time-averaged temperature.

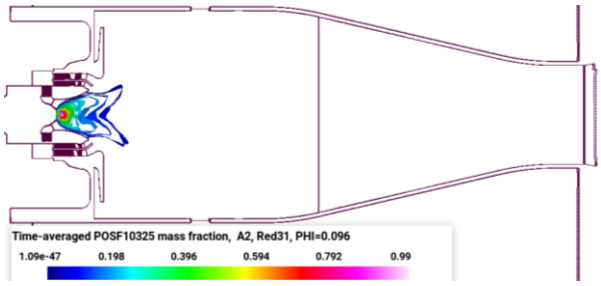

Figure 13 Time-averaged Cat-A2(POSF10325) mass fraction in a central z-normal slab cut.

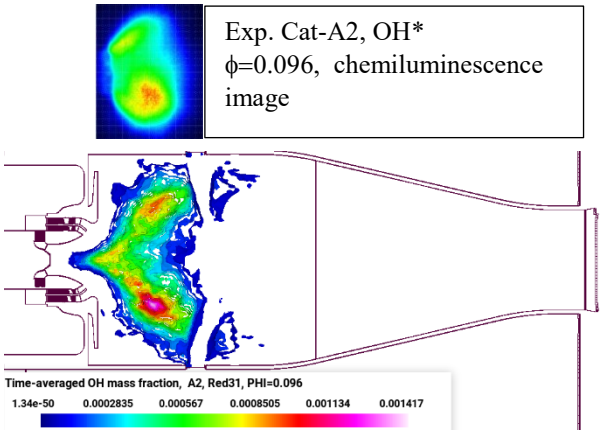

Figure 14 Experimental OH* chemiluminescence versus averaged LES OH mass fraction. (OH* is not available from LES predictions)

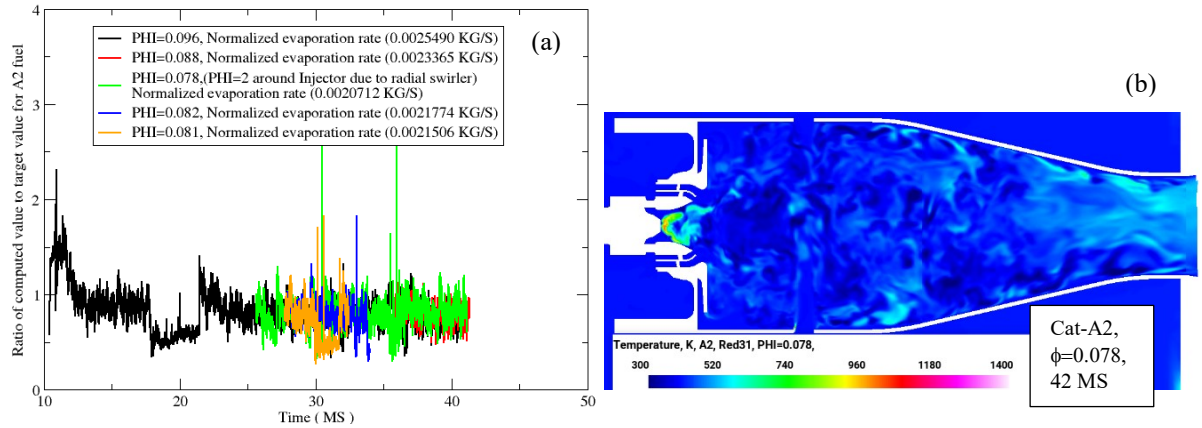

Figure 15 (a) Temporal efficiency of Cat-A2 fuel evaporations of various equivalence ratios. (b) Instantaneous temperature contours with ϕ=0.078, at 42 MS.

In Figure 16, temporal efficiency of A2-fuel heat release rates of five equivalence ratios are shown. The unsteady heat release rates of the equivalence ratios 0.078, 0.081 and 0.082 are all reduced to near zero. However, the unsteady heat release rates of the equivalence ratios 0.088 and 0.096 are hovering around the targeted values. It is projected here that the threshold equivalence ratio of the near blow-out and lean blow-out locates between 0.088 and 0.082.

In Figure 17, the temporal comparisons of normalized heat release rate and normalized T4 of A2 fuel at ϕ=0.096 are shown. Since both normalized values are all at 80%, it shows that the temperature at the

combustor exit is consistent with the heat generated in the combustor.

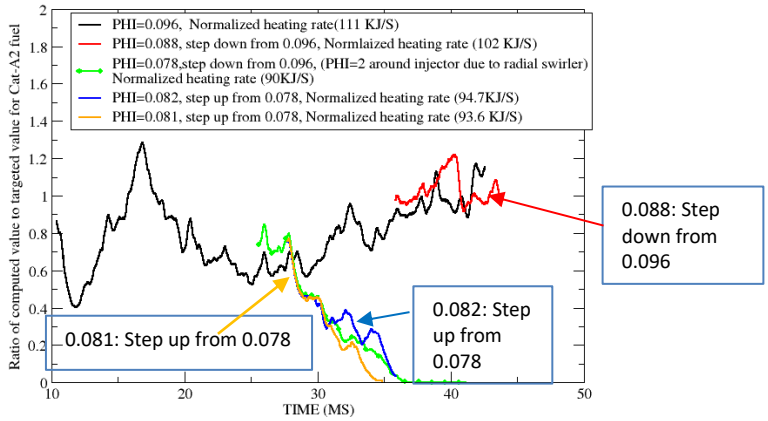

Figure 16 Temporal efficiency of A2-fuel heat release rates of various equivalence ratios.

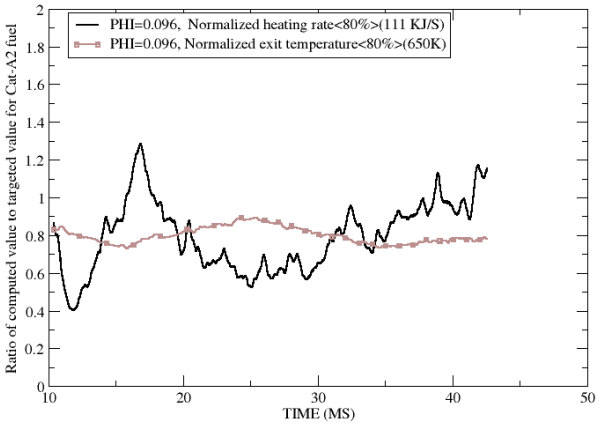

Figure 17 Temporal comparisons of normalized heat release rate and normalized T4 of Cat-A2 fuel at ϕ=0.096.

The flow split between the three swirlers and the two rows of the dilution holes is computed and is shown in Figure 18. The total mass flow of all three swirlers that enters the forward combustor is about 18.24 % of the inlet mass which is larger than that of 15.9% of the inlet mass for the non-reacting case. The effective equivalence ratio from all the swirler flowrate is about 0.53. The primary equivalence ratio from the swirler flowrate, a quarter of the first dilution jet flowrate and the dome effusive cooling flowrate is around 0.38. The total mass flowrate of all two dilution rows that enter the combustor, forward and aft, is 24.06% of the inlet mass which is larger than that of the non-reacting mass flow, 22.4% of the inlet mass.
In Figure 19, the normalized temporal evolutions of mass at inlet and at outlet are shown. The relative errors, 0.29% and 2.89%, are acceptable.

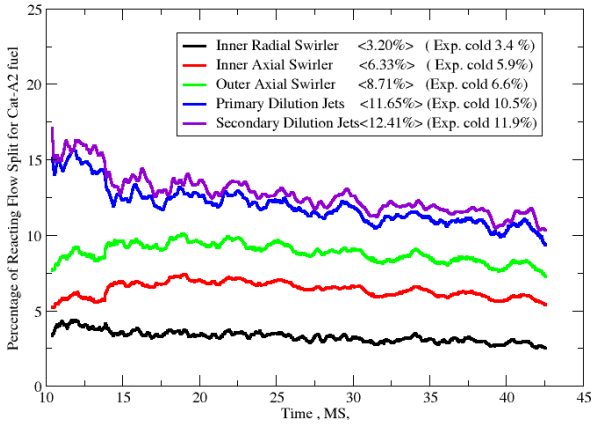

Figure 18 Temporal evolution of reacting mass flow split through three swirlers and two dilution holes of A2 fuel at ϕ=0.096.

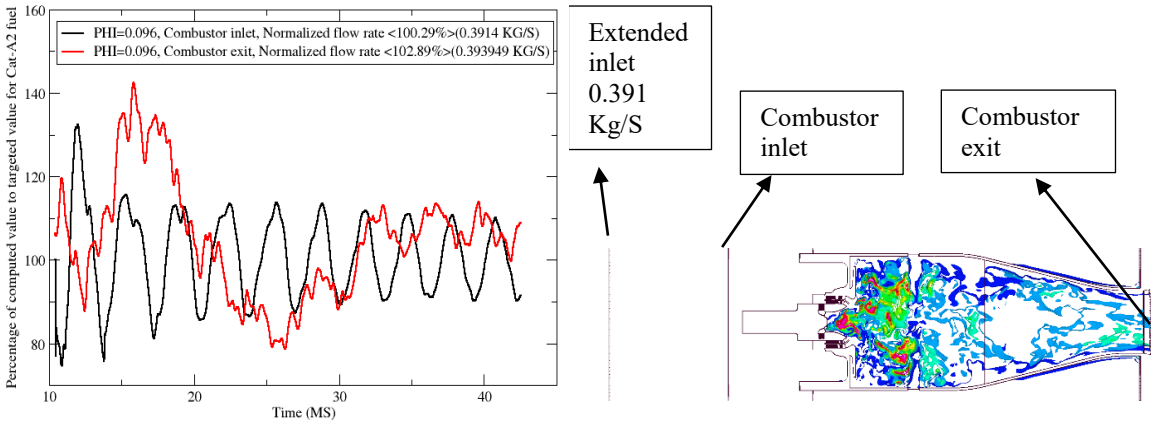

Figure 19 Temporal evolution of mass at inlet and at outlet of Cat-A2 fuel at ϕ=0.096.

Case 3. Reacting flow simulations: Cat-C1 as the fuel

The air related boundary conditions used in this case are the same as Case 1 and Case 2.

The overall equivalence ratio selected for Cat-C1 fuel is also 0.096. It is a rather steady operating condition reported from the experimental data.
The averaged formula of the Cat-C1 (Designation of POSF11498) is represented by $C_{12.6}H_{27.2}$.
A reduced hybrid chemistry (Hychem) model[7] is used for the mechanism of the real Cat-C1 fuel. The non-stiff version of the reduced mechanism consists of 26 species and 182 reactions for the purpose of lowering the cost of the finite chemistry simulations.

The liquid boundary conditions are the same as the Case 2.
The liquid properties are prescribed from T. Edward experimental database [5,6] that includes the density, heat capacity, viscosity and latent heat of vaporization, shown in Table 3. The gas properties are prescribed from H. Wang's HyChem model [7].

A middle slab cut of time-averaged axial velocity and averaged axial recirculation velocity are shown in the left and right panels of Figure 20. In Figure 21, the time-averaged transverse velocity on a middle slab cut Is shown. The bending of the dilution jets is noticeable.

From Figures 22 to 24, the contours of time-averaged K-LES speed, pressure and temperature in a central

slab cut normal to the z axis are shown respectively. The higher speed accelerated in the exit area of the aft-combustor could be contributed due to the chemical mechanism used. The pressure distribution in the aft-combustor compartment is quite uniform. The temperature distribution in the combustor is somewhat unsymmetrical and one higher temperature zone exists in lower portion of the combustor. The values of the temperature drop very quickly from the first row of the dilution hole to the second row of the dilution hole.

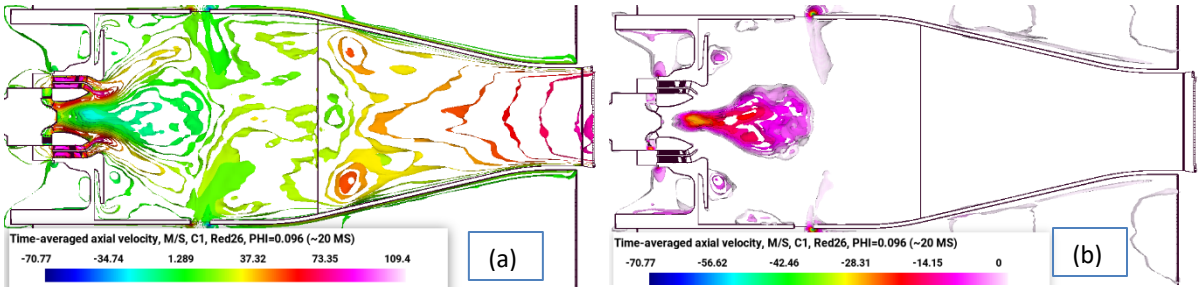

Figure 20 A middle slab cut of (a) time averaged axial velocity and (b) time averaged axial recirculation velocity of Cat-C1 fuel at ϕ=0.096.

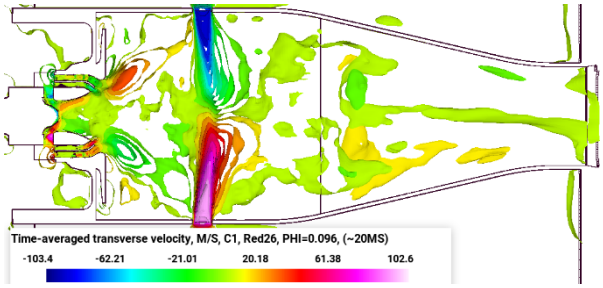

Figure 21 A middle slab cut of averaged transverse velocity.

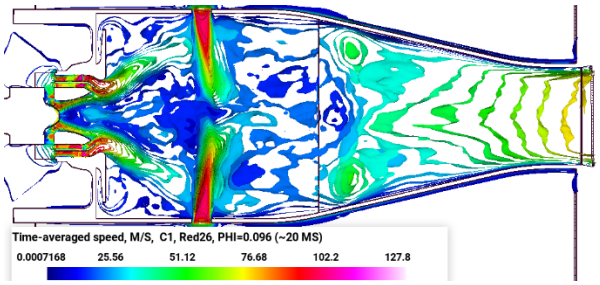

Figure 22 Velocity magnitude in a central z-normal slab cut.

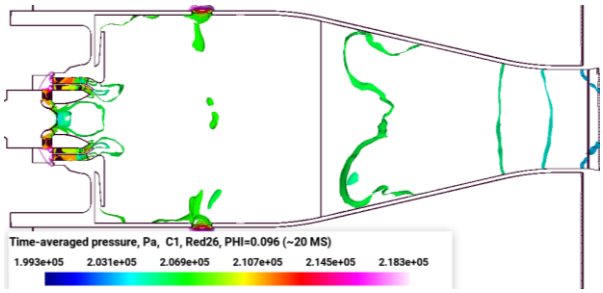

Figure 23 A middle slab cut of averaged pressure

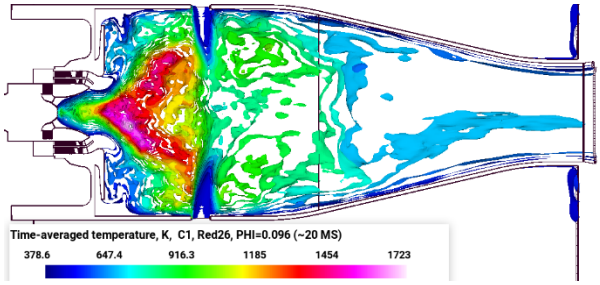

Figure 24 A middle slab cut of time-averaged temperature

The time-averaged C1 mass fraction is shown in Figure 25. It shows that the injected liquid fuel is mainly vaporized in the swirler cup due to well organized recirculation zone shown in the right panel of Figure 20. The time-averaged OH mass fraction is shown in Figure 26. Temporal efficiencies of C1 fuel evaporations, heating rate and T4 for ϕ=0.096 are shown in Figure 27 respectively. The evaporation rate for ϕ=0.096 is stable and close to the injected rate, 0.002549 kg/s.

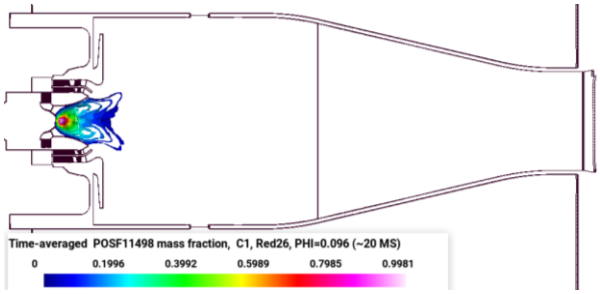

Figure 25 Time-averaged C1(POSF11498) mass fraction in a central z-normal slab cut.

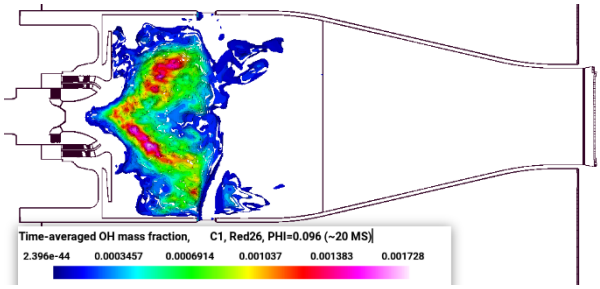

Figure 26 Time-averaged LES OH mas fraction. (OH* is not available from LES predictions)

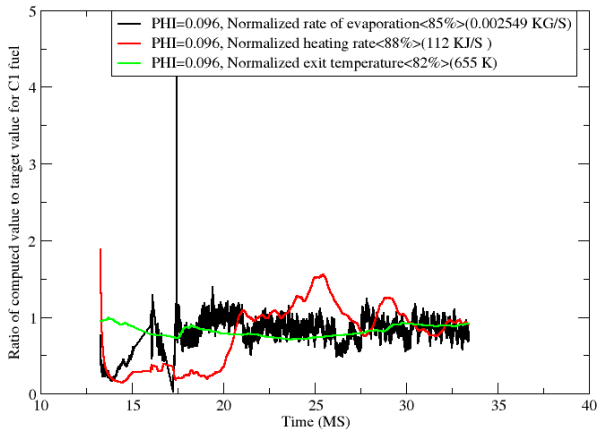

Figure 27 Temporal efficiency of Cat-C1 fuel evaporations, heating rate and T4 at ϕ=0.096

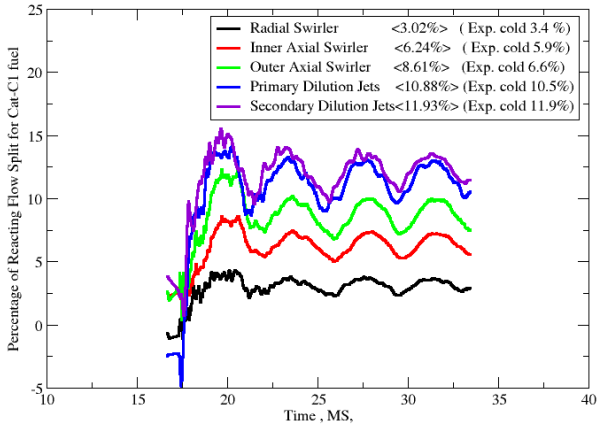

Figure 28 Temporal evolution of reacting mass flow split through three swirlers and two dilution holes.

The flow split between the three swirlers and the two rows of the dilution holes is computed. The total mass flow of all three swirlers that enters the forward combustor is about 17.87 % of the inlet mass which is larger than that of 15.9% of the inlet mass for the non-reacting case. The effective equivalence ratio from all the swirler flowrate is about 0.54. The primary equivalence ratio from the swirler flowrate, a quarter of the first dilution jet flowrate and the dome effusive cooling flowrate is around 0.4. The total mass flowrate of all two dilution rows that the enter the combustor, forward and aft, is about 22.81% of the inlet mass which is slightly more than that of 22.4% of the inlet mass for the non-reacting case.

Concluding Remarks

In this paper, the strategy of using K-LES in analyzing the sensibility of two aviation fuels in a referee combustor rig which is a single-cup, swirl-stabilized RQL (rich-burn, quick-mix, lean-burn) combustor is developed.

A non-reacting case using the same benchmark boundary conditions as the experiment is investigated with TFNS approach on a patched grid of 12640138 hexahedrons. The numerical solutions moderately predict the non-reacting flow field in terms of the profiles of mean flow split.

For the reacting cases, an average jet fuel (denoted as “Cat-A2” in the NJFCP) and a test fuel (Cat-C1) are selected for the sensitivity study.

Five calculations for Cat-A2 fuel with consecutive decreased equivalence ratios were performed to examine

the combustion characteristics starting at stable conditions near lean blow-out to lean blow-out in order to understand the trend of the stabilization mechanisms.

Only one calculation for Cat-C1 fuel was performed due to the constraint of the time. The simulations of Cat-C1 fuel indicated that at ϕ=0.096 the temperature fields were at sustainable conditions.

The simulations of Cat-A2 fuel indicated that at ϕ=0.096 and ϕ=0.088 the temperature fields were at sustainable conditions. At ϕ=0.078, which was stepped down from ϕ=0.096, the values of the unsteady heat release rate reduced to near zero in roughly 10 MS. After 2 MS stepped down from ϕ=0.096, the equivalence ratio was stepped up from 0.078 to 0.082 and 0.081. After another 8 MS, both the 0.082 and 0.081 cases approached the blow out, i.e. the unsteady heat release rates were almost zero. It is projected that the threshold of the near blow out and lean blow for the Cat-A2 fuel would be between ϕ=0.088 and ϕ=0.082 based on the value of the unsteady heat release rate.

For the future work, the capability of LES and different spray conditions in analyzing the sensibility of more aviation fuels on stable combustion conditions near blow-out and lean blow-out approaching will be investigated.

Acknowledgements

This work was supported by the NASA Transformational Tools and Technologies (TTT) project under the Transformative Aeronautics Concepts (TACP) program.

References

[1] Stouffer, Scott, et. al, "Lean Blowout and Ignition Characteristics of Conventional and Surrogate Fuels Measured in a Swirl Stabilized Combustor", *55th AIAA Aerospace Sciences Meeting*. AIAA-2017-1954.
[2] Colket, M., "An overview of the National Jet Fuels Combustion Program", *54th AIAA Aerospace Sciences Meeting*, AIAA-2016-0177.
[3] Edwards, T., "Reference Jet Fuels for Combustion Testing", *55th AIAA Aerospace Sciences Meeting*. AIAA-2017-0146.
[4]Kitamura, K, et. al, "A New Pressure Flux for AUSM-Faloly Scheme for Hypersonic Heating Computations," 2010 AIAA Computation Fluid Dynamics Conference, AIAA 2011-3030.
[5] Frossling, N., "ber die Verdunstung Fallender Tropfen," Gerlands Beitrge zur Geophysik, Vol. 52, 1938, pp.170-215.
[6] Faeth, G. M. "Evaporation and Combustion of Sprays," Prog. in Energy and Comb. Sci., 9,1 (1983)
[7] Esclapez, L., Ma, P. C., Mayhew, E., xu, R., Stouffer, S., Lee, T., Wang, H., Ihme, M., "Fuel Effects on Lean Blow-Out in a Realistic Gas Turbine Combustor," Combustion and Flame 181 (2017) 82-99.
[8]Wang, H., Xu, R., Wang, K., Bowman, C. T., Davidson, D.F., Hanson, R. K., Brezinsky, K., Egolfopoulos, F. N., "A physics-based approach to modeling real-fuel combustion chemistry - I. Evidence from experiments, and thermodynamic, chemical kinetic and statistical considerations," Combustion and Flame 193 (2018) 502-519.